Advanced Journal of Chemistry, Section A

Journal homepage: www.ajchem-a.com

Original Research Article

Effect of Calcination Temperature on the Structure of Evolution of Al-Co Co-Doped ZnO Nanofibers for High Performance Piezoelectric Energy Harvesting

Ade Irvan Tauvana[1,2], Gunawarman Gunawarman[1,*], Yuli Yetri[3], Bambang Wahono[4]

[1]*Department of Mechanical Engineering, Universitas Andalas, Kampus Limau Manis, Padang 25163, Indonesia*
[2]*Department of Manufacturing Engineering Technology, Politeknik Engineering Indorama, Purwakarta 41152, Indonesia*
[3]*Department of Mechanical Engineering, Politeknik Negeri Padang, Padang 25163, Indonesia*
[4]*National Research and Innovation Agency (BRIN), Bandung, Indonesia*

ARTICLEINFO

Article history

Submitted: 2025-12-24
Revised: 2026-01-30
Accepted: 2026-02-12
ID: AJCA-2512-2012
DOI: 10.48309/AJCA.2026.568339.2012

KEYWORDS

ZnO nanofibers
Al–Co co-doping
Electrospun nanostructures
Crystallite size
Piezoelectric energy harvesting

ABSTRACT

The development of high-efficiency piezoelectric nanogenerators (PENGs) requires nanostructured materials with controlled crystallinity, optimized morphology, and enhanced lattice stability. However, systematic investigations on Al–Co co-doped electrospun ZnO nanofibers for piezoelectric energy harvesting remain limited. This study aims to examine the effects of aluminum (Al) and cobalt (Co) co-doping on the structural, morphological, and chemical characteristics of electrospun ZnO nanofibers. ZnO nanofiber membranes were fabricated via electrospinning using PVA, ZnAc, $AlCl_3$, and CoAc precursors, followed by calcination at 500 °C. XRD results showed that Al-ZnO (100:0) exhibited the largest crystallite size (93.09 nm) and highest crystallinity, while the Al–Co (75:25) composition produced the smallest crystallites (59.52 nm) due to Co-induced lattice strain. FTIR spectra further confirmed dopant–lattice interactions through characteristic metal–oxygen vibrations. SEM analysis revealed uniform bead-free fibers with diameters ranging from 77 to 219 nm, with smoother surfaces observed in co-doped samples. EDX confirmed the successful incorporation and homogeneous distribution of Al and Co within the ZnO matrix. The results demonstrate that Al–Co co-doping effectively tunes crystallite size, crystallinity, and fibre morphology, offering a promising strategy for optimizing electrospun ZnO nanofibers toward enhanced piezoelectric energy harvesting applications.

* Corresponding author: Gunawarman, Gunawarman
✉ E-mail: gunawarman@eng.unand.ac.id

GRAPHICAL ABSTRACT

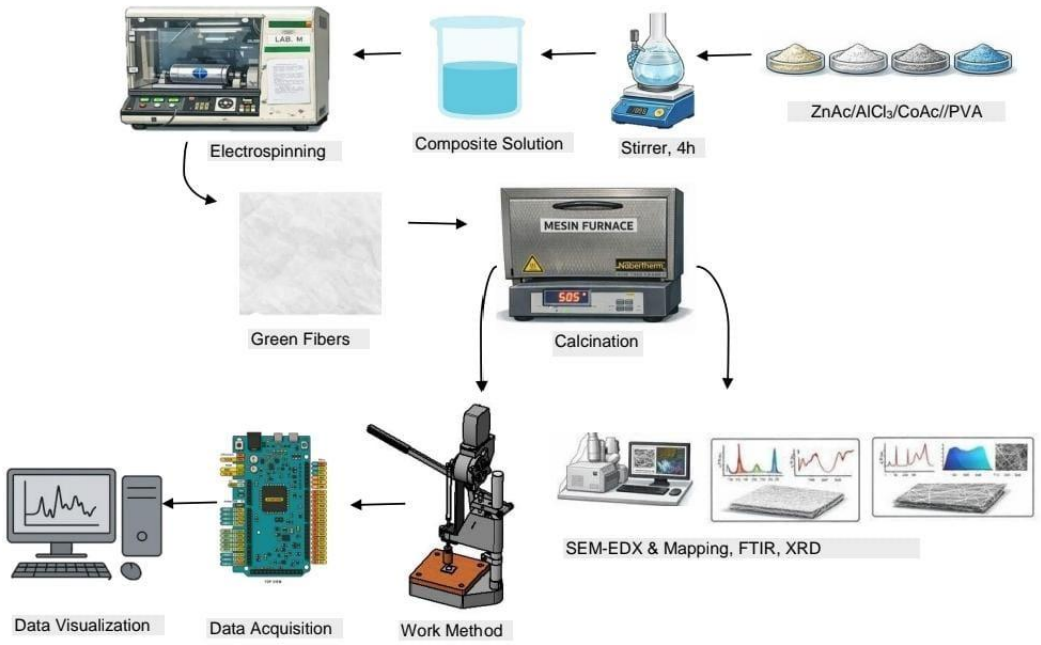

Introduction

Zinc oxide (ZnO) is a piezoelectric material that has been extensively researched for energy harvesting applications due to its relatively wide bandgap of 3.37 eV and high exciton binding energy of approximately 60 meV, which enable strong optoelectronic and electromechanical reactions [1-4]. Due to these inherent qualities, ZnO is extremely appealing for piezoelectric nanogenerators (PENGs), particularly in flexible, low-power, and micro-scale energy systems [5-7].

One-dimensional (1D) ZnO nanostructures, including nanowires, nanorods, and nanofibers, have drawn a lot of interest because of their advantageous polarization orientation under mechanical deformation, high surface-area-to-volume ratio, and enhanced stress transmission efficiency [8-10]. ZnO nanofibers provide unique benefits among these topologies, such as mechanical flexibility, continuous charge transport channels, and large-area fabrication compatibility [11-13]. As a result, electrospun ZnO nanofibers have become attractive options for PENG applications that require excellent performance. Despite these benefits, pristine ZnO still has a number of inherent drawbacks, such as restricted spontaneous polarization, low carrier mobility, and a high defect density (such as oxygen vacancies and zinc interstitials) [14-16]. These elements considerably lower the mechanical-to-electrical energy conversion efficiency in ZnO-based PENGs. To address these challenges, metal-ion doping has been thoroughly investigated as a successful method to modify the structural, electrical, and piezoelectric characteristics of ZnO [17-19].

Aluminum (Al) doping has been shown to improve crystal quality, prevent defect development, and boost carrier concentration by replacing Zn^{2+} sites with Al^{3+} ions [20-22]. The electronic band structure is altered, and lattice distortion is introduced by cobalt (Co) doping, which can increase local polarization and piezoelectric strain [23]. Nevertheless, single-doping methods frequently include built-in trade-

offs. While Co doping can increase strain, it may cause defect formation or structural instability at higher concentrations; Al doping mainly increases crystallinity but causes little lattice strain [24-26].

According to recent studies, Al–Co co-doping can produce a synergistic effect in which Co causes controlled lattice distortion that increases local polarization while Al stabilizes the ZnO lattice and enhances carrier mobility. Reports published between 2023 and 2025 indicate that dual-doped ZnO systems can enhance PENG output voltage by approximately 40–70% through improved crystallinity, reduced defect density, and optimized lattice strain [27-29]. However, despite the increasing interest in co-doping techniques, there are still relatively few systematic research on Al–Co co-doped ZnO nanofibers made by electrospinning [29-31]. Specifically, the connections between dopant distribution, crystallinity, crystallite size, fiber shape, fiber diameter, and dopant composition have not been fully explained. Electrospinning is a straightforward, scalable, and economical method that can produce continuous nanofibers with regulated diameters and good dopant uniformity, making it especially suitable for fabricating doped ceramic and metal oxide nanofibers [32-34]. Previous research has demonstrated that the morphology and diameter distribution of electrospun ZnO-derived nanofibers are significantly influenced by precursor chemistry, dopant concentration, and electrospinning parameters [35-37]. Consequently, electrospinning offers a perfect platform for methodically examining whether co-doping affects ZnO nanofiber microstructure. In this study, ZnO nanofibers with varying Al–Co co-doping compositions were synthesized via electrospinning, followed by calcination, to systematically evaluate the effects of co-doping on fiber morphology, diameter, crystallinity, crystallite size, and microstructure. This work aims to establish a fundamental understanding of the structure–property relationships in Al–Co co-doped ZnO nanofibers and to clarify the underlying mechanisms responsible for performance enhancement in ZnO-based piezoelectric nanogenerators [18].

Materials and Methods

Materials

Zinc acetate dihydrate ($Zn(CH_3COO)_2{\cdot}2H_2O$, Merck), aluminum chloride hexahydrate ($AlCl_3{\cdot}6H_2O$, Merck), cobalt acetate tetrahydrate ($Co(CH_3COO)_2{\cdot}4H_2O$, Sigma-Aldrich), polyvinyl alcohol (PVA, Mw ≈ 72,000, Merck), and deionized water were used as received without further purification. These precursors were selected based on their high solubility in aqueous media, chemical stability, and compatibility with polymer-assisted electrospinning processes, making them suitable for the fabrication of ZnO-based nanofibers

Preparation of nanofiber precursor solutions

A 10 wt% PVA solution was prepared by dissolving PVA powder in deionized water at 70 °C under continuous stirring for 4 h. The solution was subsequently aged at room temperature for 8 h to ensure complete dissolution and homogenization. For the synthesis of doped ZnO systems, 3.6 g of ZnO was dispersed in 20 mL of deionized water under constant stirring, followed by the gradual addition of 0.4 g of aluminum or cobalt precursor to obtain Al-doped ZnO or Co-doped ZnO, respectively. The reaction mixture was maintained under heating and continuous stirring to ensure homogeneous dispersion, while the reaction vessel was sealed to minimize solvent evaporation and contamination. Subsequently, the Zn-based precursor solution was mixed with the PVA solution at a ratio corresponding to approximately 4 wt% PVA relative to the inorganic phase. To investigate the effect of co-doping composition, two precursor solutions, namely ZnO–Al and ZnO–Co, were separately prepared at a fixed dopant concentration and subsequently mixed at Al:Co weight ratios were detailed in Table 1. These ratios represent the mixing proportions of the respective precursor solutions rather than the direct addition of

metallic dopants, thereby maintaining a constant total dopant content while systematically varying the relative contribution of Al^{3+} and Co^{2+} ions. The resulting mixtures were stirred at elevated temperatures until a uniform and stable ZnO–PVA composite suspension was obtained, and subsequently used as the base solutions for the electrospinning process.

Electrospinning process

Electrospinning was conducted using a 5 mL plastic syringe mounted on a syringe pump and fitted by a stainless-steel needle with an inner diameter of 0.65 mm. A high-voltage power supply was connected to the needle tip, while nanofibers were collected on a nonwoven membrane attached to a rotating drum collector.

The electrospinning parameters were fixed at an applied voltage of 13 kV, a tip-to-collector distance of 13 cm, a solution flow rate of 0.5 mL h^{-1}, and a drum rotation speed of 125 rpm. The relative humidity during electrospinning was maintained at approximately 58%. These parameters were selected to obtain uniform and bead-free nanofibers.

Calcination process

The electrospun nanofiber membranes were calcined in a muffle furnace at 500 °C for 3 h with a heating rate of 2 °C min^{-1}. This thermal treatment was conducted to ensure complete decomposition of the PVA matrix and conversion of the precursor into crystalline ZnO nanofibers. The selected calcination temperature has been reported to effectively promote crystallization while preserving the fibrous morphology of electrospun ZnO nanofibers.

Characterization of nanofiber membranes

Crystallographic analysis was carried out using X-ray diffraction (XRD) to identify phase formation, evaluate crystallinality, and estimate crystallite size using the Scherrer equation, which is widely applied to doped ZnO nanostructures. Fourier transform infrared (FTIR) spectroscopy was employed to investigate chemical bonding and dopant–lattice interactions by analyzing shifts in Zn–O vibrational modes and the appearance of dopant-related absorption bands [25]. The morphology, fiber uniformity, and diameter distribution of the nanofiber membranes were subsequently examined using scanning electron microscopy (SEM), while the elemental composition and dopant distribution were analyzed by energy-dispersive X-ray spectroscopy (EDX).

Results and Discussion

Structural and functional group analysis

The XRD patterns of all samples, depicted in Figure 1, exhibit diffraction peaks characteristic of the hexagonal wurtzite ZnO structure, with the dominant reflections corresponding to the (100), (002), and (103) planes located at $2\theta \approx 31–33°$, 34–36°, and 47–49°, respectively, in good agreement with the JCPDS card No. 36-145 [38]. No secondary phases related to Al- or Co-based oxides were detected, indicating successful dopant incorporation into the ZnO lattice within the detection limit of XRD.

Table 1. Zn-based precursor solution variation

Sample	ZnO-Al solution	ZnO-Co solution
A	100	0
B	75	25
C	50	50
D	25	75
E	0	100

Variations in peak intensity and peak width are observed with changes in the $AlCl_3$/CoAc ratio, suggesting modifications in crystallinity and lattice strain. The sample with 100% $AlCl_3$ (Al-doped ZnO) shows the highest intensity of the (002) reflection, indicating a pronounced preferential orientation along the c-axis and relatively high crystallinity. This behavior is consistent with previous reports that Al^{3+} substitution for Zn^{2+} can promote c-axis texture due to its smaller ionic radius and stronger ionic bonding, which enhances lattice packing. With increasing Co content, a gradual decrease in peak intensity accompanied by slight peak broadening is observed, particularly for samples with Al–Co ratios of 50:50 and higher Co fractions. This trend indicates increased lattice distortion and microstrain, attributed to the difference in ionic radius between Co^{2+} and Zn^{2+} and the resulting local structural disorder. Nevertheless, the persistence of the wurtzite ZnO peaks across all compositions confirms that the overall crystal structure remains stable despite dopant-induced lattice perturbations. The crystallite size and crystallinity values listed in Table 2 show a clear nonlinear trend across Samples A–E. Sample A exhibits the largest crystallite size of 93.09 nm with a crystallinity of 78.78%, indicating highly developed crystal domains. A substantial decrease of approximately 36% in crystallite size is observed for Sample B (59.52 nm), accompanied by a comparable crystallinity level (78.99%), suggesting that initial dopant incorporation significantly suppresses crystallite growth without severely disrupting long-range order. From Sample B to Sample D, the crystallite size increases progressively from 59.52 nm to 85.05 nm, corresponding to an increase of about 43%, while crystallinity remains within a narrow range (74.16–78.99%). This trend indicates partial lattice relaxation and dopant-assisted recrystallization within the wurtzite structure. Sample E exhibits a moderate crystallite size of 79.81 nm with a crystallinity of 77.75%, reflecting a balance between lattice distortion and structural stability.

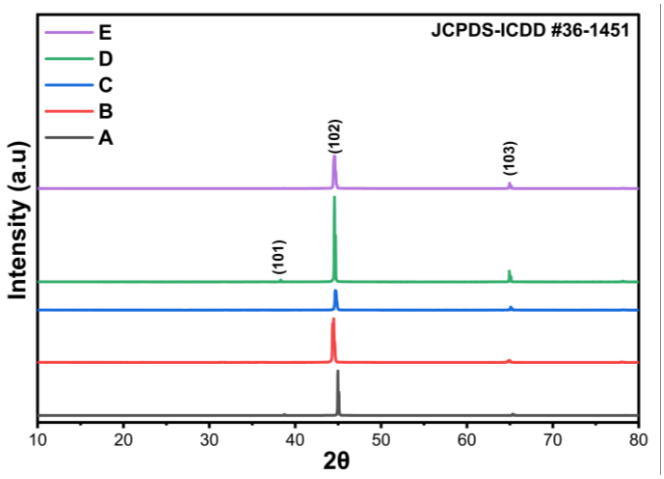

Figure 1. XRD analysis of Al–Co co-doped ZnO nanofibers after calcination

Table 2. Crystallite size and degree of crystallinity of the samples

Sample	Crystallite size (nm)	Crystallinity (%)
A	93.09	78.78
B	59.52	78.99
C	79.56	74.16
D	85.05	74.43
E	79.81	77.75

Overall, the quantitative evolution of crystallite size and crystallinity across Samples A–E demonstrates a competition between crystallite growth inhibition at lower compositional stability and structural recovery at intermediate to higher compositions, highlighting the role of dopant interactions in modulating crystal domain evolution within electrospun ZnO nanofibers. Three-dimensional structural modeling using VESTA software, constructed from XRD data, confirms that all doped ZnO nanofibers retain the characteristic hexagonal wurtzite structure with space group $P6_3mc$. In the model, Zn atoms are tetrahedrally coordinated by oxygen atoms within a dense hexagonal lattice, while Al and Co atoms substitute Zn sites due to their comparable ionic radii as depicted in Figure 2. Although the global crystal symmetry remains intact, dopant incorporation induces localized lattice strain, which is consistent with the observed peak broadening and crystallite size variations.

Overall, the XRD analysis demonstrates that Al–Co co-doping effectively modulates the crystallographic characteristics of ZnO nanofibers through a synergistic interplay between crystal growth promotion (Al^{3+}) and lattice distortion (Co^{2+}). This controlled tuning of crystallinity and lattice strain is expected to influence the electronic structure, carrier mobility, and piezoelectric response, thereby reinforcing the suitability of Al–Co co-doped ZnO nanofibers for piezoelectric nanogenerator applications.

FTIR analysis was employed to investigate the bonding characteristics and defect-related features of Al–Co co-doped ZnO nanofibers after calcination. All samples exhibit a dominant absorption band in the range of 450 to 520 cm^{-1}, which is assigned to the Zn–O stretching vibration of the hexagonal wurtzite ZnO lattice, confirming the successful formation of crystalline ZnO [39]. As shown in Figure 3, samples with higher Al content display a relatively sharper and more intense Zn–O band, indicating stronger metal–oxygen bonding and improved lattice regularity. In contrast, increasing Co content leads to slight band broadening and reduced intensity, suggesting enhanced lattice distortion and local strain induced by the substitution of Co^{2+} ions with a larger ionic radius into the ZnO matrix.

Additional weak absorption bands observed at approximately 1,380–1,450 cm^{-1} are attributed to C–O stretching vibrations, while the band near ~1,630 cm^{-1} corresponds to O–H bending modes. Furthermore, a broad absorption region in the range of 3,200–3,600 cm^{-1} is associated with O–H stretching vibrations originating from surface hydroxyl groups and adsorbed moisture [40]. The relative intensity of these defect-related bands increases progressively with increasing Co content, indicating a higher density of surface adsorption sites and defect states. This trend is consistent with the XRD results, which reveal reduced crystallinity and increased microstrain for Co-rich compositions.

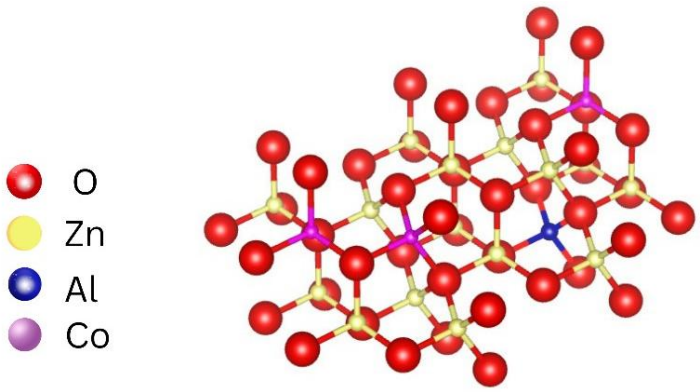

Figure 2. Structural model of ZnO doped with Co and Al, demonstrating lattice modification induced by dopant incorporation

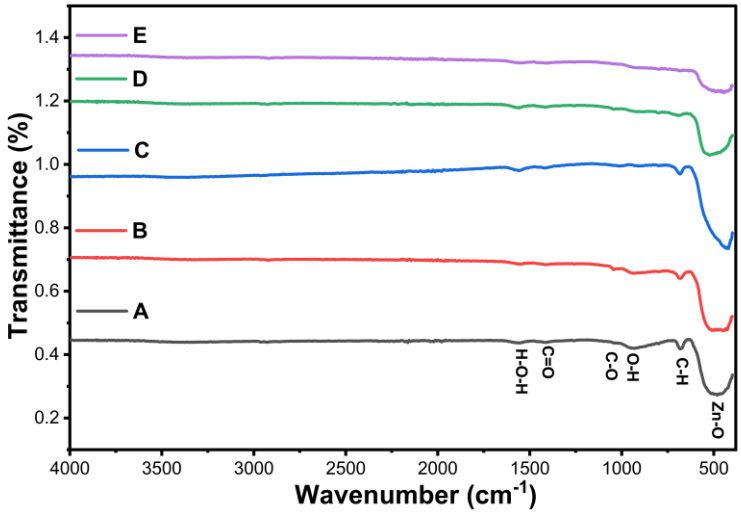

Figure 3. FTIR analysis of Al–Co co-doped ZnO nanofibers after calcination

From a functional perspective, a moderate presence of surface hydroxyl groups and lattice defects can enhance surface polarization and facilitate dipole reorientation under mechanical deformation, contributing positively to piezoelectric energy harvesting. However, excessive defect concentration, as suggested by the stronger O–H- and C–O-related absorption features at higher Co compositions may disrupt long-range lattice coherence and reduce effective polarization. Therefore, samples exhibiting an optimal balance between Zn–O bond integrity and controlled defect density are expected to demonstrate superior piezoelectric performance. Overall, the FTIR results corroborate the structural trends observed in XRD analysis and confirm that Al–Co co-doping effectively modulates bond structure, defect chemistry, and functional properties of electrospun ZnO nanofibers. SEM micrographs of electrospun ZnO nanofibers co-doped with $AlCl_3$ and CoAc at $AlCl_3$ compositions of 100, 75, 50, 25, and 0%, after calcination at 500 °C for 3 h, are presented in Figure 4. The calcination process induces significant fiber shrinkage and polymer decomposition, leading to the formation of crystalline ZnO nanofibers with distinct morphological features that strongly depend on the Al–Co dopant ratio [41]. This morphological evolution is consistent with the measured nanofiber diameter distribution, indicating a close relationship between dopant composition, thermal stability, and fiber densification behavior.

The Al-rich nanofibers exhibit smooth, continuous, and relatively homogeneous morphologies, with well-defined fibrous networks and minimal surface irregularities. These samples show the most stable average diameters and narrower minimum–maximum diameter ranges, suggesting that Al^{3+} ions effectively stabilize the ZnO lattice during high-temperature calcination. The substitution of Zn^{2+} by Al^{3+} is known to suppress excessive lattice distortion and defect formation, thereby promoting uniform shrinkage and preserving fiber integrity. As a result, Al-dominated compositions display superior morphological uniformity and structural stability after calcination. With increasing Co content, a gradual transition toward rougher and more irregular fiber morphologies is observed. At intermediate Al–Co ratios, the nanofibers begin to exhibit surface wrinkling and noticeable diameter variations along the fiber length, indicating uneven shrinkage during thermal treatment. This behavior can be attributed to Co^{2+} incorporation, which introduces lattice strain due to differences in ionic radius and bonding characteristics relative to Zn^{2+}. The presence of Co-induced lattice distortion reduces thermal stability,

leading to non-uniform densification and increased morphological heterogeneity. At high Co concentrations, the nanofibers display pronounced surface roughness, irregular thickness, and local fiber fusion at junction points, accompanied by a broader diameter distribution. These features indicate excessive lattice strain and reduced resistance to thermal stress during calcination, resulting in uneven crystallite growth and morphological degradation. The fully Co-doped sample exhibits the highest degree of structural irregularity, confirming that excessive Co incorporation negatively impacts fiber uniformity and post-calcination stability. Overall, the SEM analysis clearly demonstrates that the Al–Co co-doping ratio plays a critical role in governing the morphological evolution of electrospun ZnO nanofibers. Increasing Co content leads to greater fiber shrinkage variability, surface wrinkling, and morphological inconsistency, whereas Al-rich compositions promote smoother surfaces, narrower diameter, distributions, enhancing structural stability. These findings highlight the complementary roles of Al and Co dopants, where Al acts as a lattice stabilizer and Co induces controlled lattice distortion, and are in good agreement with previous studies on doped electrospun ZnO nanofibers [26,27]. The observed morphology–composition relationship provides an important foundation for understanding the subsequent crystallographic and functional properties of Al–Co co-doped ZnO nanofibers. The statistical analysis of fiber diameter, as presented in Figure 4**,** reveals clear variations in the average fiber diameter among all samples. Sample A exhibits the smallest average fiber diameter of 0.07744 µm (~77 nm), indicating effective jet stretching and fine fiber formation. Sample C and sample D show comparable average diameters of 0.10352 µm (~104 nm) and 0.1092 µm (~109 nm), respectively, suggesting relatively stable electrospinning conditions with moderate fiber thickening. In contrast, samples B and E display significantly larger average fiber diameters, reaching 0.1978 µm (~198 nm) for sample B and 0.21856 µm (~219 nm) for sample E. These larger diameters are accompanied by broader diameter distributions, as observed in the corresponding histograms, indicating increased jet instability, fiber merging, or reduced elongational forces during electrospinning. This behaviour is consistent with the SEM images, where samples B and E show thicker fibers and more irregular fibrous networks. Among all samples, sample C demonstrates the most balanced fiber characteristics, combining a moderate average diameter with a relatively narrow and symmetric diameter distribution. This confirms that the optimized $AlCl_3$/CoAc ratio promotes stable electrospinning conditions. Such diameter uniformity is particularly crucial for piezoelectric nanofibers, as it enables consistent mechanical deformation and contributes to a more reliable electrical response under applied mechanical stress. The elemental compositions of samples A–E obtained from EDX analysis are presented in Table 3. The results indicate a clear compositional trend as a function of $AlCl_3$/CoAc ratio. As the Al content increases from sample A to E, the Zn content decreases significantly, suggesting partial substitution of Zn^{2+} ions by Al^{3+} within the ZnO lattice or competitive incorporation during fiber formation. Despite the variation in precursor composition, the Co content remains relatively low and stable across all samples (0.47–1.84 wt%), indicating that Co acts primarily as a secondary dopant without significantly altering the overall lattice stoichiometry. This low and controlled Co incorporation is beneficial, as excessive Co content could induce secondary phases or structural instability. Among all compositions, sample C exhibits the most balanced Al–Zn ratio, with moderate Al content (51.63 wt%) and the highest Co incorporation (1.84 wt%) that remains within a stable range. This compositional balance is expected to promote lattice distortion without severe structural degradation, which is advantageous for enhancing polarization mechanisms in ZnO-based piezoelectric materials.

Table 3. The elemental composition of samples from EDX analysis

Element	Sample				
Weight %	A	B	C	D	E
O K	11.37	7.13	9.86	8.11	4.75
Al K	56.58	67.78	51.63	64.64	80.32
Co K	0.47	0.68	1.84	1.03	1.35
Zn K	31.59	24.4	36.66	26.22	13.58

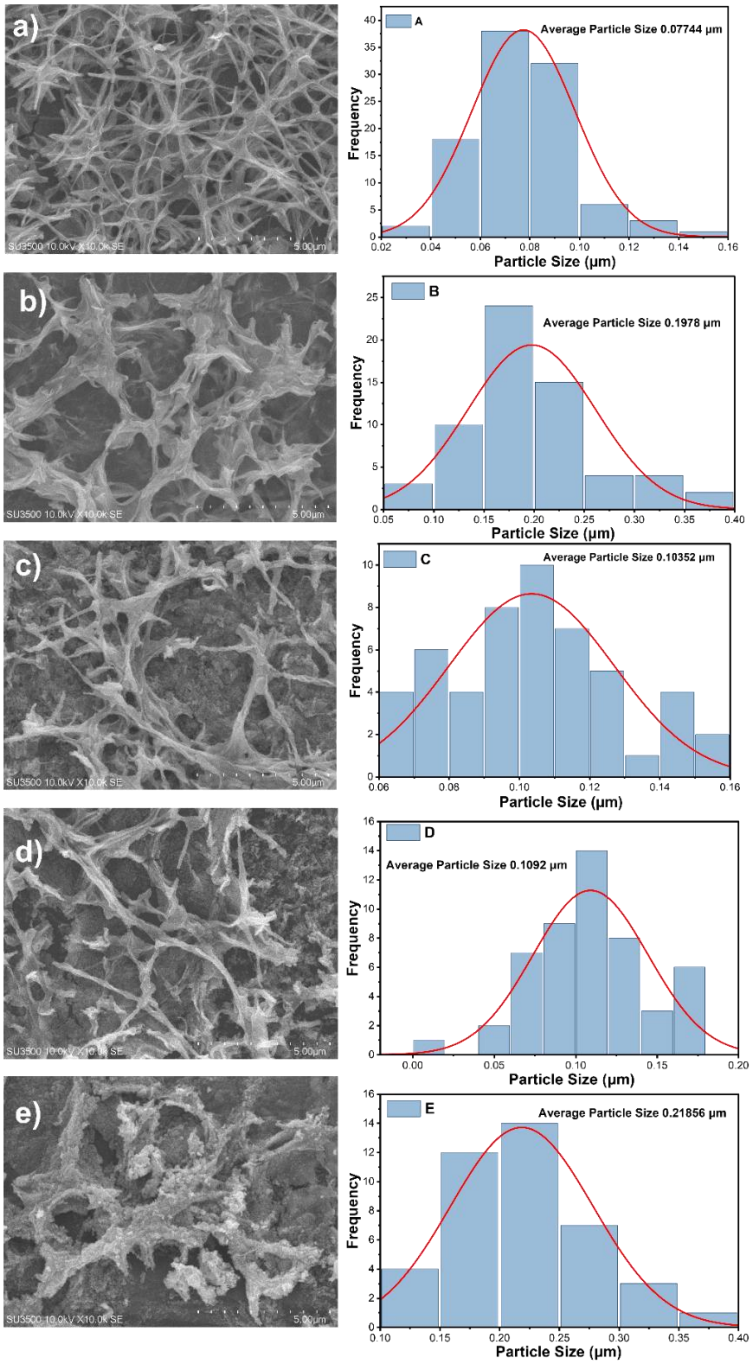

Figure 4. SEM analysis and particle size distribution of Al–Co co-doped ZnO nanofibers after calcination

Conclusion

Variations in the Al–Co doping ratio distinctly regulate the structural evolution of electrospun ZnO nanofibres, where XRD reveals Al-driven crystallite growth, Co-induced lattice strain, and co-stabilization at intermediate compositions. FTIR confirms corresponding modifications in Zn–O bonding and defect-related vibrational features, and SEM demonstrates a transition from smooth, uniform fibres to increased roughness and diameter variation with higher Co content. This indicates that intermediate Al–Co compositions offer the most favorable balance of crystallinity, lattice stability, and morphology for enhanced piezoelectric nanogenerator performance.

Acknowledgements

The authors would like to sincerely acknowledge the valuable support and contributions of all parties who assisted in the completion of this research. They would also like to thank the Politeknik Enjinering Indorama for providing essential equipment used in the characterization process. This research was financially supported by the PDD program funding from DPPM-DIKTISAINTEK under contract DIPA no. 139.04.1.693320/2025.

Conflict of Interest

No conflict of interest was reported by the authors in this work.

ORCID

Ade Irvan Tauvana:
https://orcid.org/0000-0003-0470-4307
Gunawarman Gunawarman:
https://orcid.org/0000-0002-2291-5514
Yuli Yetri:
https://orcid.org/0000-0002-3349-4081
Bambang Wahono:
https://orcid.org/0000-0002-4172-4254

References

[1] Bhadwal, N., Ben Mrad, R., Behdinan, K. Review of zinc oxide piezoelectric nanogenerators: Piezoelectric properties, composite structures and power output. *Sensors*, **2023**, 23(8), 3859.
[2] Kumar, B., Kim, S.-W. Energy harvesting based on semiconducting piezoelectric ZnO nanostructures. *Nano Energy*, **2012**, 1(3), 342–355.
[3] Jin, C., Zhou, J., Wu, Z., Zhang, J.X. Doped zinc oxide-based piezoelectric devices for energy harvesting and sensing. *Advanced Energy and Sustainability Research*, **2025**, 6(9), 2500017.
[4] Özgür, Ü., Alivov, Y.I., Liu, C., Teke, A., Reshchikov, M.A., Doğan, S., Avrutin, V., Cho, S.-J., Morkoç. A comprehensive review of ZnO materials and devices. *Journal of Applied Physics*, **2005**, 98(4).
[5] Wang, Z.L., Song, J. Piezoelectric nanogenerators based on zinc oxide nanowire arrays. *Science*, **2006**, 312(5771), 242–246.
[6] Razack, R.K., Sadasivuni, K.K. Advancing nanogenerators: The role of 3D-printed nanocomposites in energy harvesting. *Polymers*, **2025**, 17(10), 1367.
[7] Cai, X., Wang, Y., Cao, Y., Yang, W., Xia, T., Li, W. Flexural-mode piezoelectric resonators: Structure, performance, and emerging applications in physical sensing technology, micropower systems, and biomedicine. *Sensors*, **2024**, 24(11), 3625.
[8] Raha, S., Ahmaruzzaman, M. ZnO nanostructured materials and their potential applications: Progress, challenges and perspectives. *Nanoscale Advances*, **2022**, 4(8), 1868–1925.
[9] Weintraub, B., Zhou, Z., Li, Y., Deng, Y. Solution synthesis of one-dimensional ZnO nanomaterials and their applications. *Nanoscale*, **2010**, 2(9), 1573–1587.
[10] Janotti, A., Van de Walle, C.G. Fundamentals of zinc oxide as a semiconductor. *Reports on Progress in Physics*, **2009**, 72(12), 126501.
[11] Long, Y.-Z., Yu, M., Sun, B., Gu, C.-Z., Fan, Z. Recent advances in large-scale assembly of semiconducting inorganic nanowires and nanofibers for electronics, sensors and photovoltaics. *Chemical Society Reviews*, **2012**, 41(12), 4560–4580.
[12] Rong, P., Ren, S., Yu, Q. Fabrications and applications of ZnO nanomaterials in flexible functional devices-a review. *Critical Reviews in Analytical Chemistry*, **2019**, 49(4), 336–349.
[13] Look, D.C. Recent advances in ZnO materials and devices. *Materials Science and Engineering: B*, **2001**, 80(1-3), 383–387.
[14] Sharma, D.K., Shukla, S., Sharma, K.K., Kumar, V. A review on ZnO: Fundamental properties and

applications. *Materials Today: Proceedings*, **2022**, 49, 3028–3035.
[15] Kozuka, Y., Tsukazaki, A., Kawasaki, M. Challenges and opportunities of ZnO-related single crystalline heterostructures. *Applied Physics Reviews*, **2014**, 1(1).
[16] Borysiewicz, M.A. ZnO as a functional material, a review. *Crystals*, **2019**, 9(10), 505.
[17] Jin, C., Hao, N., Xu, Z., Trase, I., Nie, Y., Dong, L., Closson, A., Chen, Z., Zhang, J.X. Flexible piezoelectric nanogenerators using metal-doped ZnO-PVDF films. *Sensors and Actuators A: Physical*, **2020**, 305, 111912.
[18] Kumari, P., Misra, K.P., Chattopadhyay, S., Samanta, S. A brief review on transition metal ion doped ZnO nanoparticles and its optoelectronic applications. *Materials Today: Proceedings*, **2021**, 43, 3297–3302.
[19] Luo, Z., Rong, P., Yang, Z., Zhang, J., Zou, X., Yu, Q. Preparation and application of Co-doped zinc oxide: A review. *Molecules*, **2024**, 29(14), 3373.
[20] Sharma, H.K., Archana, R., Singh, B.P., Ponnusamy, S., Hayakawa, Y., Muthamizhchelvan, C., Raji, P., Kim, D.Y., Sharma, S.K. Substitution of Al^{3+} to Zn^{2+} sites of ZnO enhanced the photocatalytic degradation of methylene blue under irradiation of visible light. *Solid State Sciences*, **2019**, 94, 45–53.
[21] de Lara Andrade, J., Oliveira, A.G., Mariucci, V.V.G., Bento, A.C., Companhoni, M.V., Nakamura, C.V., Lima, S.M., da Cunha Andrade, L.H., Moraes, J.C.G., Hechenleitner, A.A.W., Pineda, E.A.G. Effects of Al^{3+} concentration on the optical, structural, photocatalytic and cytotoxic properties of Al-doped ZnO. *Journal of Alloys and Compounds*, **2017**, 729, 978-987.
[22] Kalyani, C., Reddy, I.S., Raju, P., Raju, P.M.S. Effects of Al^{3+} concentration on the structural, dielectric and conductivity properties of al-doped ZnO. *Materials Today: Proceedings*, **2023**, 80, 1111–1115.
[23] Zheng, M.-P., Hou, Y.-D., Xie, F.-Y., Chen, J., Zhu, M.-K., Yan, H. Effect of valence state and incorporation site of cobalt dopants on the microstructure and electrical properties of 0.2 PZN–0.8 PZT ceramics. *Acta Materialia*, **2013**, 61(5), 1489–1498.
[24] Fang, D., Lin, K., Xue, T., Cui, C., Chen, X., Yao, P., Li, H. Influence of al doping on structural and optical properties of Mg–Al co-doped ZnO thin films prepared by sol–gel method. *Journal of Alloys and Compounds*, **2014**, 589, 346–352.
[25] Yue, X., Dong, Y., Cao, H., Wei, X., Zheng, Q., Sun, W., Lin, D. Effect of electronic structure modulation and layer spacing change of NiAl layered double hydroxide nanoflowers caused by cobalt doping on supercapacitor performance. *Journal of Colloid and Interface Science*, **2023**, 630, 973–983.
[26] Benzarti, Z., Saadi, H., Abdelmoula, N., Hammami, I., Graça, M.P.F., Alrasheedi, N., Louhichi, B., de Melo, J.S.S. Enhanced dielectric and photocatalytic properties of Li-doped zno nanoparticles for sustainable methylene blue degradation with reduced lithium environmental impact. *Ceramics International*, **2025**, 51(25), 47170–47184.
[27] Kim, I., Yun, J., Kim, G., Kim, D. Triboelectric-enhanced piezoelectric nanogenerator with pressure-processed multi-electrospun fiber-based polymeric layer for wearable and flexible electronics. *Polymers*, **2025**, 17(17), 2295.
[28] Rehman, N.U., Khan, R., Rahman, N., Ahmad, I., Ullah, A., Sohail, M., Iqbal, S., Althubeiti, K., Al Otaibi, S., Juraev, N. Dual-doped ZnO-based magnetic semiconductor resistive switching response for memristor-based technologies. *Journal of Materials Science: Materials in Electronics*, **2024**, 35(23), 1557.
[29] Sagar, P., Sinha, N., Kumar, B. Hydrothermally grown pure and Er-doped ZnS nanocrystals based flexible piezoelectric nanogenerator for energy harvesting and sensing applications. *Journal of Crystal Growth*, **2024**, 632, 127646.
[30] Singh, M., Scotognella, F. Recent progress in solution processed aluminum and co-doped ZnO for transparent conductive oxide applications. *Micromachines*, **2023**, 14(3), 536.
[31] Acar, Y., Coban, M.B., Gungor, E., Dogan, M., Turhan, Y. Spectroscopic and morphological properties of white light emitted electrospun PVA @ ZnO : x Dy^{3+} nanofibers. *Reactive and Functional Polymers*, **2025**, 217, 106463.
[32] Esfahani, H., Jose, R., Ramakrishna, S. Electrospun ceramic nanofiber mats today: Synthesis, properties, and applications. *Materials*, **2017**, 10(11), 1238.
[33] Banitaba, S.N., Ehrmann, A. Application of electrospun nanofibers for fabrication of versatile and highly efficient electrochemical devices: A review. *Polymers*, **2021**, 13(11), 1741.
[34] Cho, Y., Baek, J.W., Sagong, M., Ahn, S., Nam, J.S., Kim, I.D. Electrospinning and nanofiber technology: Fundamentals, innovations, and applications. *Advanced Materials*, **2025**, 37(28), 2500162.
[35] Blachowicz, T., Ehrmann, A. Recent developments in electrospun ZnO nanofibers: A short review. *Journal of Engineered Fibers and Fabrics*, **2020**, 15, 1558925019899682.
[36] Nazhipkyzy, M., Maltay, A.B., Seilkhanov, T.M. Synthesis of carbon nanofibers from lignin using nickel for supercapacitor applications. *Fibers*, **2024**, 12(10), 87.
[37] Habis, C., Colin, B., Jimenez, C., Michel, S., Aillerie, M. Specific role of al in the synthesis of electrospun Al: ZnO nanofibers: Thermal and elemental

analysis. *Materials Today Communications*, **2024**, 38, 108196.
[38] Sedefoglu, N. Characterization and photocatalytic activity of ZnO nanoparticles by green synthesis method. *Optik*, **2023**, 288, 171217.
[39] Abdelkrim, M., Guezzoul, M.h., Bedrouni, M., Bouslama, M.h., Ouerdane, A., Kharroubi, B. Effect of slight cobalt incorporation on the chemical, structural, morphological, optoelectronic, and photocatalytic properties of ZnO thin film. *Journal of Alloys and Compounds*, **2022**, 920, 165703.
[40] Dai, F., Zhuang, Q., Huang, G., Deng, H., Zhang, X. Infrared spectrum characteristics and quantification of oH groups in coal. *ACS Omega*, **2023**, 8(19), 17064–17076.
[41] Yun, S., Lim, S. Effect of Al-doping on the structure and optical properties of electrospun zinc oxide nanofiber films. *Journal of Colloid and Interface Science*, **2011**, 360(2), 430–439.

HOW TO CITE THIS ARTICLE

A.I. Tauvana, G. Gunawarman, Y. Yetri, B. Wahono. Effect of Calcination Temperature on the Structure of Evolution of Al-Co Co-Doped ZnO Nanofibers for High Performance Piezoelectric Energy Harvesting. *Adv. J. Chem. A*, 2026, 9(7), 1297-1308.

DOI: 10.48309/AJCA.2026.568339.2012
URL: https://www.ajchem-a.com/article_240604.html